

# Higher Order Fluctuations and Correlations of Conserved Charges from Lattice QCD

S. Borsanyi, Z. Fodor, J. N. Guenther

published in

## **NIC Symposium 2020**

M. Müller, K. Binder, A. Trautmann (Editors)

Forschungszentrum Jülich GmbH,  
John von Neumann Institute for Computing (NIC),  
Schriften des Forschungszentrums Jülich, NIC Series, Vol. 50,  
ISBN 978-3-95806-443-0, pp. 207.  
<http://hdl.handle.net/2128/24435>

© 2020 by Forschungszentrum Jülich

Permission to make digital or hard copies of portions of this work for personal or classroom use is granted provided that the copies are not made or distributed for profit or commercial advantage and that copies bear this notice and the full citation on the first page. To copy otherwise requires prior specific permission by the publisher mentioned above.

# Higher Order Fluctuations and Correlations of Conserved Charges from Lattice QCD

Szabolcs Borsanyi<sup>1</sup>, Zoltan Fodor<sup>1,2,3</sup>, and Jana N. Guenther<sup>1,4</sup>

<sup>1</sup> University of Wuppertal, 42119 Wuppertal, Germany  
*E-mail: fodor@physik.uni-wuppertal.de*

<sup>2</sup> Eötvös University, 1117 Budapest, Hungary

<sup>3</sup> Jülich Supercomputing Centre, 52425 Jülich, Germany

<sup>4</sup> University of Regensburg, 93053 Regensburg, Germany

We calculate several diagonal and non-diagonal fluctuations of conserved charges in a system of  $2+1+1$  quark flavours with physical masses, on a lattice with size  $48^3 \times 12$ . Higher order fluctuations at  $\mu_B = 0$  are obtained as derivatives of the lower order ones, simulated at imaginary chemical potential. From these correlations and fluctuations we construct ratios of net-baryon number cumulants as functions of temperature and chemical potential, which satisfy the experimental conditions of strangeness neutrality and proton/baryon ratio. Our results qualitatively explain the behaviour of the measured cumulant ratios by the STAR collaboration.

## 1 Introduction

One of the most challenging goals in the study of Quantum Chromodynamics (QCD) is a precise mapping of the phase diagram of strongly interacting matter. First principle, lattice QCD simulations predict that the transition from hadrons to deconfined quarks and gluons is a smooth crossover, taking place in the temperature range  $T \simeq 145 - 165$  MeV. Lattice simulations cannot presently be performed at finite density due to the sign problem, thus leading to the fact that the QCD phase diagram is still vastly unexplored when the asymmetry between matter and antimatter becomes large.

With the advent of the second Beam Energy Scan (BES-II) at the Relativistic Heavy Ion Collider (RHIC), scheduled for 2019-2020, there is a renewed interest in the heavy ion community towards the phases of QCD at moderate-to-large densities. A rich theoretical effort is being developed in support of the experimental program; several observables are being calculated, in order to constrain the existence and location of the QCD critical point and to observe it experimentally.

Fluctuations of conserved charges (electric charge  $Q$ , baryon number  $B$  and strangeness  $S$ ) are among the most relevant observables for the finite-density program for several reasons. One possible way to extend lattice results to finite density is to perform Taylor expansions of the thermodynamic observables around chemical potential  $\mu_B = 0$ . Recent results can be found in Ref. 1. Fluctuations of conserved charges are directly related to the Taylor expansion coefficients of such observables, thus, they are needed to extend first principle approaches to the regions of the phase diagram relevant to RHIC. An other popular method to extend observables to finite density is the analytical continuation from imaginary chemical potentials. The agreement between the analytical continuation and Taylor expansion was shown for the transition temperature by Bonati *et al.* in Ref. 2.

Fluctuations can also be measured directly, and a comparison between theoretical and experimental results allows to extract the chemical freeze-out temperature  $T_f$  and chemical potential  $\mu_{Bf}$  as functions of the collision energy. Such fluctuations have been recently calculated and extrapolated using the Taylor method in Ref. 3. Finally, higher order fluctuations of conserved charges are proportional to powers of the correlation length and are expected to diverge at the critical point, thus providing an important signature for its experimental detection.<sup>4</sup>

In this project, we calculate several diagonal and non-diagonal fluctuations of conserved charges up to sixth-order and give estimates for higher orders, in the temperature range  $135 \text{ MeV} \leq T \leq 220 \text{ MeV}$ , for a system of 2+1+1 dynamical quarks with physical masses and lattice size  $48^3 \times 12$ . We simulate the lower-order fluctuations at imaginary chemical potential and extract the higher order fluctuations as derivatives of the lower order ones at  $\mu_B = 0$ . This method has been successfully used in the past and proved to lead to a more precise determination of the higher order fluctuations, compared to their direct calculation.<sup>5,6</sup> The direct method (see *e. g.* Ref. 7) requires the evaluation of several terms and is affected by a signal-to-noise ratio which is decreasing as a power law of the spatial volume  $V$ , with an exponent that grows with the order of the susceptibility.

We also construct combinations of these diagonal and non-diagonal fluctuations in order to study the ratio of the cumulants of the net-baryon number distribution as functions of temperature and chemical potential by means of their Taylor expansion in powers of  $\mu_B/T$ . We discuss their qualitative comparison with the experimental results from the STAR collaboration, as well as the validity of the truncation of the Taylor series.

## 2 Fluctuations and Imaginary Chemical Potentials

The chemical potentials are implemented on a flavour-by-flavour basis, their relation to the phenomenological baryon ( $B$ ), electric charge ( $Q$ ) and strangeness ( $S$ ) chemical potentials are given by

$$\mu_u = \frac{1}{3}\mu_B + \frac{2}{3}\mu_Q, \quad \mu_d = \frac{1}{3}\mu_B - \frac{1}{3}\mu_Q, \quad \mu_s = \frac{1}{3}\mu_B - \frac{1}{3}\mu_Q - \mu_S \quad (1)$$

The observables we are looking at are the derivatives of the free energy with respect to the chemical potentials. Since the free energy is proportional to the pressure, we can write:

$$\chi_{i,j,k}^{B,Q,S} = \frac{\partial^{i+j+k}(p/T^4)}{(\partial\hat{\mu}_B)^i(\partial\hat{\mu}_Q)^j(\partial\hat{\mu}_S)^k} \quad (2)$$

with  $\hat{\mu}_i = \frac{\mu_i}{T}$ . These are the generalised fluctuations we calculated around  $\mu = 0$  in our previous work.<sup>8</sup>

The fermion determinant  $\det M(\mu)$  is complex for real chemical potentials, prohibiting the use of traditional simulation algorithms. For imaginary  $\mu$ , however, the determinant stays real. The chemical potential is introduced through weighted temporal links in the staggered formalism:  $U_0(\mu) = e^\mu U_0$  and  $U_0^\dagger(\mu) = e^{-\mu} U_0^\dagger$ . Thus, an imaginary  $\mu$  translates into a phase factor for the antiperiodic boundary condition in the Dirac operator. Due to the  $Z(3)$  symmetry of the gauge sector, there is a non-trivial periodicity in the imaginary quark chemical potential  $\mu_q \rightarrow \mu_q + i(2\pi/3)T$ , which translates to the baryochemical potential as  $\mu_B \rightarrow \mu_B + i2\pi T$ , the Roberge-Weiss symmetry. This is independent of the charge conjugation symmetry  $\mu_B \leftrightarrow -\mu_B$ .

At  $\mu_B = i\pi T$  there is a first order phase transition at all temperatures above the Roberge-Weiss critical end point  $T_{RW}$ .<sup>9</sup> When  $\mu_B$  crosses  $i\pi T$  in the imaginary direction, the imaginary baryon density is discontinuous. At low temperature the Hadron Resonance Gas model predicts  $\langle B \rangle \sim \sinh(\mu_B/T)$ , thus for imaginary values we expect a sine function below  $T_c$ :  $\text{Im}\langle B \rangle \sim \sin(\text{Im}\mu_B/T)$ . At temperatures slightly above  $T_c$ , we observe that further Fourier components appear in addition to  $\sin(\text{Im}\mu_B/T)$  with alternating coefficients, these are consistent with a repulsive interaction between baryons.<sup>10</sup> At very high temperatures, on the other hand,  $\langle B \rangle$  is a polynomial of  $\mu_B$  since the diagrams contributing to its  $\sim \mu_B^5$  and higher order components are suppressed by asymptotic freedom.<sup>11</sup> The Stefan-Boltzmann limit is non-vanishing only for two Taylor coefficients of  $\text{Im}\langle B \rangle$ , giving  $\text{Im}\langle B \rangle|_{\mu_B/T=i\pi-\epsilon} = 8\pi/27$ . At finite temperatures above  $T_{RW}$  this expectation value is smaller but positive, which implies a first order transition at  $\mu_B = i\pi T$ .

We have only the range  $\mu/T \in [0, i\pi)$  to explore the  $\mu$ -dependence of the observables. Recent simulations in this range include the determination of the transition line, where the slope was determined on the negative side of the  $T - \mu_B^2$  phase diagram. Using analyticity arguments, this coefficient gives the curvature of the transition line on the real  $T - \mu_B$  phase diagram.<sup>12-14</sup> Apart from the transition temperature, we used imaginary chemical potentials also to extrapolate the equation of state to real  $\mu_B$ ,<sup>5</sup> which serves as an alternative approach to the Taylor extrapolation.<sup>15</sup> In a recent study D’Elia *et al.* have used the low order fluctuations at imaginary chemical potentials to calculate generalised quark number susceptibilities.<sup>6</sup>

### 3 Analysis Details

#### 3.1 Lattice Setup

In this work we calculate high order fluctuations by studying the imaginary chemical potential dependence of various generalised quark number susceptibilities.

We use a tree-level Symanzik improved gauge action, with four times stout smeared ( $\rho = 0.125$ ) staggered fermions. We simulate  $2 + 1 + 1$  dynamical quarks, where the light flavours are tuned in a way to reproduce the physical pion and kaon masses and we set  $\frac{m_c}{m_s} = 11.85$ .<sup>16</sup> For the zero-temperature runs that we used for the determination of the bare masses and the coupling, the volumes satisfy  $Lm_\pi > 4$ . The scale is determined via  $f_\pi$ . More details on the scale setting and lattice setup can be found in Ref. 8.

Our lattice ensembles are generated at eighteen temperatures in the temperature range 135...220 MeV. We simulate at eight different values of imaginary  $\mu_B$  given as:  $\mu_B^{(j)} = iT \frac{j\pi}{8}$  for  $j \in \{0, 1, 2, 3, 4, 5, 6, 7\}$ . In this work the analysis is done purely on a  $48^3 \times 12$  lattice, we leave the continuum extrapolation for future work.

In terms of quark chemical potentials we generate ensembles with  $\mu_u = \mu_d = \mu_s = \mu_B/3$ . In each simulation point we calculate all derivatives in Eq. 2 up to fourth order. Thanks to our scan in  $\text{Im}\hat{\mu}_B$ , we can calculate additional  $\mu_B$  derivatives. Ref. 6 uses various “trajectories” in the  $\mu_B - \mu_Q - \mu_S$  space, allowing the numerical determination of higher *e.g.*  $\mu_Q$  and  $\mu_S$  derivatives. We find a relatively good signal for the  $\mu_Q$  and  $\mu_S$  derivatives by directly evaluating Eq. 2 within one simulation. We recently summarised the details of the direct calculation in Ref. 8.

### 3.2 Correlated Fit with Priors

We start with the analysis for  $\chi_2^B(T)$ ,  $\chi_4^B(T)$  and  $\chi_6^B(T)$ . Our goal is to calculate these quantities at zero chemical potential, using the imaginary chemical potential data up to  $\chi_B^4(T, \hat{\mu}_B)$ . In this work we extract these derivatives at a fixed temperature. Results for different temperatures are obtained completely independently, an interpolation in temperature is not necessary at any point. Thus, the error bars in our results plot will be independent. The errors between the quantities  $\chi_2^B(T)$ ,  $\chi_4^B(T)$  and  $\chi_6^B(T)$  will be highly correlated, though, since these are extracted through the same set of ensembles at the given temperature. This correlation will be taken into account when combined quantities are calculated, or when an extrapolation to real chemical potential is undertaken.

Thus we consider the ensembles at a fixed temperature  $T$ . For each value of imaginary  $\mu_B \neq 0$  we determine  $\chi_1^B$ ,  $\chi_2^B$ ,  $\chi_3^B$  and  $\chi_4^B$  from simulation, while for  $\mu_B = 0$  only  $\chi_2^B$  and  $\chi_4^B$  can be used, since  $\chi_1^B$  and  $\chi_3^B$  are odd functions of  $\mu_B$  and therefore equal to zero.

We make the following ansatz for the pressure:

$$\chi_0^B(\hat{\mu}_B) = c_0 + c_2\hat{\mu}_B^2 + c_4\hat{\mu}_B^4 + c_6\hat{\mu}_B^6 + c_8\hat{\mu}_B^8 + c_{10}\hat{\mu}_B^{10} \quad (3)$$

where the Taylor expansion coefficients  $c_n$  are related to the baryon number fluctuations  $\chi_n^B$  by:  $n!c_n = \chi_n^B$ . Our data do not allow for an independent determination of  $c_8$  and  $c_{10}$ . Nevertheless, in order to have some control over these terms we make assumptions on the higher order terms. A detailed discussion on our assumptions can be found in Ref. 17. In the fit function we keep the terms up to  $\chi_{10}^B = 10!c_{10}$ . Without this term the statistical errors on  $\chi_8^B$  were clearly smaller, but the fit would be less controlled. As the highest order in the function, the resulting  $\chi_{10}^B$  probably contains severe contamination from even higher order terms. For this reason, and since we fit  $\chi_{10}^B$  with large statistical errors we do not give results on that quantity. For simplicity, we use the same prior distribution for  $\chi_{10}^B/\chi_4^B$  as for  $\chi_8^B/\chi_4^B$ .

We can then rewrite our ansatz as

$$\chi_0^B(\hat{\mu}_B) = c_0 + c_2\hat{\mu}_B^2 + c_4\hat{\mu}_B^4 + c_6\hat{\mu}_B^6 + \frac{4!}{8!}c_4\epsilon_1\hat{\mu}_B^8 + \frac{4!}{10!}c_4\epsilon_2\hat{\mu}_B^{10} \quad (4)$$

where  $\epsilon_1$  and  $\epsilon_2$  are drawn randomly from a normal distribution with mean -1.25 and variance 2.75. We use the same distribution for all temperatures. In effect, our  $c_8$  and  $c_{10}$  coefficients are stochastic variables. The used distribution for  $\epsilon_{1,2}$  actually implements a prior for  $\chi_8^B$  and  $\chi_{10}^B$ .

For this ansatz we calculate the following derivatives, which are the actually simulated lattice observables:

$$\chi_1^B(\hat{\mu}_B) = 2c_2\hat{\mu}_B + 4c_4\hat{\mu}_B^3 + 6c_6\hat{\mu}_B^5 + \frac{4!}{7!}c_4\epsilon_1\hat{\mu}_B^7 + \frac{4!}{9!}c_4\epsilon_2\hat{\mu}_B^9 \quad (5)$$

$$\chi_2^B(\hat{\mu}_B) = 2c_2 + 12c_4\hat{\mu}_B^2 + 30c_6\hat{\mu}_B^4 + \frac{4!}{6!}c_4\epsilon_1\hat{\mu}_B^6 + \frac{4!}{8!}c_4\epsilon_2\hat{\mu}_B^8 \quad (6)$$

$$\chi_3^B(\hat{\mu}_B) = 24c_4\hat{\mu}_B + 120c_6\hat{\mu}_B^3 + \frac{4!}{5!}c_4\epsilon_1\hat{\mu}_B^5 + \frac{4!}{7!}c_4\epsilon_2\hat{\mu}_B^7 \quad (7)$$

$$\chi_4^B(\hat{\mu}_B) = 24c_4 + 360c_6\hat{\mu}_B^2 + c_4\epsilon_1\hat{\mu}_B^4 + \frac{4!}{6!}c_4\epsilon_2\hat{\mu}_B^6 \quad (8)$$

We perform a correlated fit for the four measured observables, thus obtaining the values of  $c_2$ ,  $c_4$  and  $c_6$  for each temperature, and the corresponding  $\chi_2^B$ ,  $\chi_4^B$  and  $\chi_6^B$ . We repeat

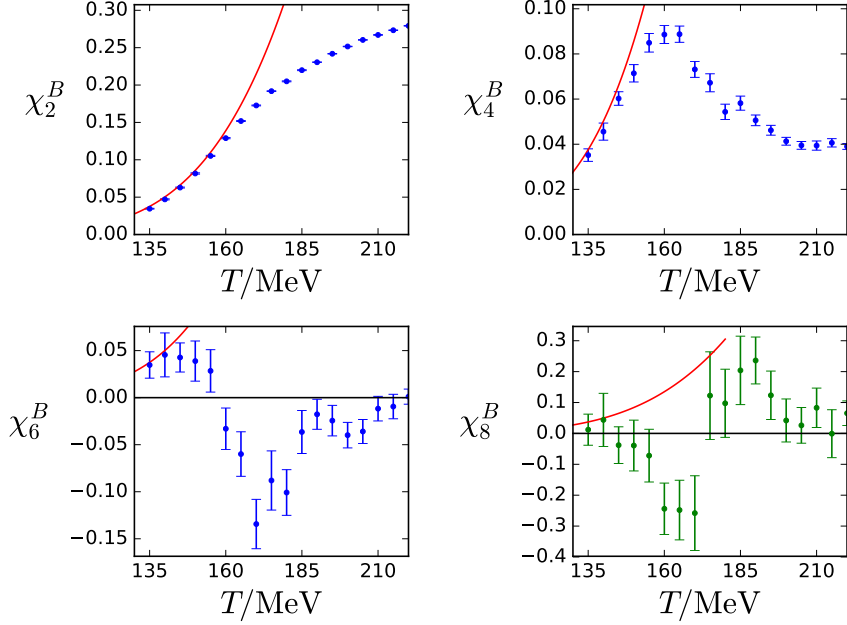


Figure 1. Results for  $\chi_2^B$ ,  $\chi_4^B$ ,  $\chi_6^B$  and an estimate for  $\chi_8^B$  as functions of the temperature, obtained from the single-temperature analysis. We plot  $\chi_8^B$  in green to point out that its determination is guided by a prior, which is linked to the  $\chi_4^B$  observable by Eq. 4. The red curve in each panel corresponds to the Hadron Resonance Gas (HRG) model result.

the fit for 1000 random draws for  $\epsilon_1$  and  $\epsilon_2$ . The result is weighted using the Akaike Information Criterion.<sup>18</sup> Through these weights we get a posterior distribution from the prior distribution. Our final estimate for  $\chi_8^B$  represents this posterior distribution. These results are shown in Fig. 1, together with an estimate of  $\chi_8^B$ , related to  $\chi_4^B$  by Eq. 4. With a similar fit procedure we determine a number of diagonal and off-diagonal fluctuations.

### 3.3 Error Analysis

For a reliable comparison between experimental measurements and theoretical calculations, the error estimate is an important ingredient. Our statistical error is estimated through the jackknife method. For our systematic error there are several sources. We determine our systematic error by the histogram method described in Ref. 19, where each analysis is weighted with the Akaike information criteria. We include the influence of the number of points in the  $\mu_B$  direction, by either including or ignoring the data from our highest value of  $\mu_B$ . A very important source for our systematic error is the influence of the higher order contributions in  $\mu_B$ . This effect was estimated by adding the higher order terms with pre-factors  $\epsilon_1$  and  $\epsilon_2$  as described in Sec. 3.2. We consider 1000 different  $\epsilon$  pairs and add the different analyses to our histogram. The width of the histogram using Akaike weights corresponding to the fit quality gives the systematic errors for the fit coefficients, and from the same histogram we obtain the posterior distributions for  $\epsilon_1$ . The physical quantities

that are constrained only by the posterior distribution are plotted with green symbols.

These histograms are built independently for each number ( $j$  and  $k$ ) of  $\mu_S$  and  $\mu_Q$  derivatives. When calculating the systematics for the cumulant ratios (Sec. 4) we need to calculate different combinations of diagonal and non-diagonal fluctuations from the available analyses. Though these fits (corresponding to the same temperature) are carried out separately we keep track of the statistical correlation, by maintaining the jackknife ensembles throughout the analysis. The correct propagation of systematic errors is a more elaborate procedure. When  $\chi_{ijk}^{BSQ}$  coefficients are combined with different  $j, k$  pairs, different histograms have to be combined. If we had only two variables to combine, each of the 2000 first fit variants should be combined with each of the 2000 second fit variants and use the product of the respective probability weights. Instead, we combine the fit results by drawing 'good' fits by importance sampling from each histogram independently. In this way,  $\mathcal{O}(100)$  random combinations of  $\chi_{ijk}^{BSQ}$  results already give convergence for each discussed quantity and its error bar. For the results in this paper we used 1000 such random combinations. This procedure assumes that between different  $j, k$  pairs the prior distribution is uncorrelated.

## 4 Phenomenology at Finite Chemical Potential

For a comparison with heavy ion collision experiments, the cumulants of the net-baryon distribution are very useful observables. The first four cumulants are the mean  $M_B$ , the variance  $\sigma_B^2$ , the skewness  $S_B$  and the kurtosis  $\kappa_B$ . By forming appropriate ratios, we can cancel out explicit volume factors. However, the measured distributions themselves may still depend on the volume, which one should take into account when comparing to experiments.

Heavy ion collisions involving lead or gold atoms at  $\mu_B > 0$  correspond to the following situation  $\langle n_S \rangle = 0$  and  $\langle n_Q \rangle = 0.4 \langle n_B \rangle$ . For each  $T$  and  $\mu_B$  pair, we have to first calculate  $\mu_Q$  and  $\mu_S$  that satisfy this condition. The resulting  $\mu_Q(\mu_B)$  and  $\mu_S(\mu_B)$  functions, too, can be Taylor expanded,<sup>20, 21</sup> introducing

$$q_j = \frac{1}{j!} \frac{d^j \hat{\mu}_Q}{(d\hat{\mu}_B)^j} \Big|_{\mu_B=0}, \quad s_j = \frac{1}{j!} \frac{d^j \hat{\mu}_S}{(d\hat{\mu}_B)^j} \Big|_{\mu_B=0} \quad (9)$$

We investigate three different ratios of cumulants:

$$\frac{M_B}{\sigma_B^2} = \frac{\chi_1^B(T, \hat{\mu}_B)}{\chi_2^B(T, \hat{\mu}_B)} = \hat{\mu}_B r_{12}^{B,1} + \hat{\mu}_B^3 r_{12}^{B,3} + \dots \quad (10)$$

$$\frac{S_B \sigma_B^3}{M_B} = \frac{\chi_3^B(T, \hat{\mu}_B)}{\chi_1^B(T, \hat{\mu}_B)} = r_{31}^{B,0} + \hat{\mu}_B^2 r_{31}^{B,2} + \dots \quad (11)$$

$$\kappa_B \sigma_B^2 = \frac{\chi_4^B(T, \hat{\mu}_B)}{\chi_2^B(T, \hat{\mu}_B)} = r_{42}^{B,0} + \hat{\mu}_B^2 r_{42}^{B,2} + \hat{\mu}_B^4 r_{42}^{B,4} + \dots \quad (12)$$

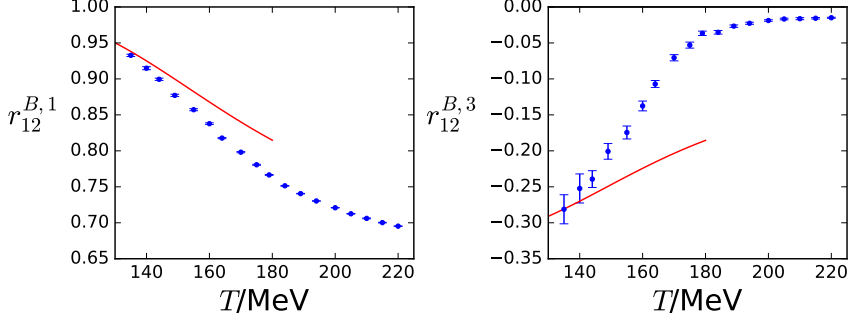


Figure 2. Taylor expansion coefficients for  $\frac{M_B}{\sigma_B^2} = \frac{\chi_1^B(T, \hat{\mu}_B)}{\chi_2^B(T, \hat{\mu}_B)}$  as functions of the temperature:  $r_{12}^{B,1}$  (left panel) and  $r_{12}^{B,3}$  (right panel).

The  $\mu_B$ -dependence of the  $\chi_i^B(T, \hat{\mu}_B)$  can again be written as a Taylor series:

$$\begin{aligned} \chi_{i,j,k}^{BQS}(\hat{\mu}_B) &= \chi_{i,j,k}^{BQS}(0) + \hat{\mu}_B \left[ \chi_{i+1,j,k}^{BQS}(0) + q_1 \chi_{i,j+1,k}^{BQS}(0) + s_1 \chi_{i,j,k+1}^{BQS}(0) \right] \\ &+ \frac{1}{2} \hat{\mu}_B^2 \left[ \chi_{i+2,j,k}^{BQS}(0) + q_1^2 \chi_{i,j+2,k}^{BQS}(0) + s_1^2 \chi_{i,j,k+2}^{BQS}(0) \right. \\ &\left. + 2q_1 s_1 \chi_{i,j+1,k+1}^{BQS}(0) + 2q_1 \chi_{i+1,j+1,k}^{BQS}(0) + 2s_1 \chi_{i+1,j,k+1}^{BQS}(0) \right] + \dots \quad (13) \end{aligned}$$

The  $\chi$  coefficients that we determined in Sec. 3 include derivatives up to sixth order, and we have estimates for the eighth order, too. The fit coefficients corresponding to the tenth order are likely to be contaminated by higher orders, that we did not include into the ansatz. These  $\chi_{ijk}^{BQS}$  coefficients, however, are given for  $j + k \leq 4$ , which is the highest order that we used in  $\mu_Q$  and  $\mu_S$ .

This list of coefficients allows us to calculate the  $r_{ij}^{B,k}$  coefficients from Eqs. 10, 11 and 12. The results for the  $r_{12}^{B,k}$  coefficients are shown in Fig. 2. We confirm the observation from Ref. 3 that the coefficient  $r_{42}^{B,2}$  has a similar temperature dependence as  $r_{31}^{B,2}$  but it is  $\sim 3$  times larger in magnitude.

For higher order coefficients, higher order derivatives in  $\mu_S$  and  $\mu_Q$  are needed. The direct simulations have a rapidly increasing error with the order of the derivative, and very large statistics would be needed to improve our calculations at this point. Another possibility would be to simulate new ensembles with finite  $\mu_S$  and  $\mu_Q$  and do a similar fit as for the  $\mu_B$  direction. This approach has been used in Ref. 6.

After calculating the Taylor coefficients for  $S_B \sigma_B^3 / M_B$  and  $\kappa_B \sigma_B^2$ , we use these results to extrapolate these quantities to finite chemical potential. They are shown in Fig. 3. In the left panel,  $S_B \sigma_B^3 / M_B$  is shown as a function of the chemical potential for different temperatures. The Taylor expansion for this quantity is truncated at  $\mathcal{O}(\hat{\mu}_B^2)$ . The black points in the figure are the experimental results from the STAR collaboration from an analysis of cumulant ratios measured at mid-rapidity,  $|y| \leq 0.5$ , including protons and anti-protons with transverse momenta  $0.4 \text{ GeV} \leq p_t \leq 2.0 \text{ GeV}$ .<sup>22,23</sup> The beam energies were translated to chemical potentials using the fitted formula of Ref. 24. Even if we do



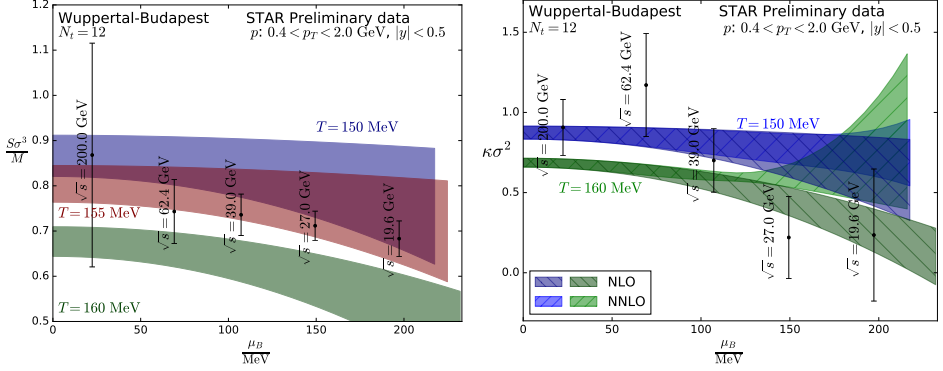


Figure 3.  $S_B \sigma_B^3 / M_B$  (left panel) and  $\kappa_B \sigma_B^2$  (right panel) extrapolated to finite chemical potential. The left panel is extrapolated up to  $\mathcal{O}(\hat{\mu}_B^2)$ . In the right panel, the darker bands correspond to the extrapolation up to  $\mathcal{O}(\hat{\mu}_B^2)$ , whereas the lighter bands also include the  $\mathcal{O}(\hat{\mu}_B^4)$  term.

not quantitatively compare the lattice bands to the measurements to extract the freeze-out parameters, as experimental higher order fluctuations might be affected by several effects of non-thermal origin and our lattice results are not continuum extrapolated, we notice that the trend of the data with increasing  $\mu_B$  can be understood in terms of our Taylor expansion.

In the right panel, we show  $\kappa_B \sigma_B^2$  as a function of  $\mu_B / T$  for different temperatures. The darker bands correspond to the extrapolation up to  $\mathcal{O}(\hat{\mu}_B^2)$ , whereas the lighter bands also include the  $\mathcal{O}(\hat{\mu}_B^4)$  term. Also in this case, the black points are the experimental results from the STAR collaboration with transverse momentum cut  $0.4 \text{ GeV} \leq p_t \leq 2.0 \text{ GeV}$ .<sup>22, 23</sup> Notice that, due to the fact that the  $r_{42}^{B,4}$  is positive in the range  $160 \text{ MeV} \leq T \leq 195 \text{ MeV}$ , we observe a non-monotonic behaviour in  $\kappa_B \sigma_B^2$  for  $T = 160 \text{ MeV}$  at large chemical potentials. By comparing the two different truncations of the Taylor series we can conclude that, as we increase the temperature, the range of applicability of our Taylor series decreases: while at  $T = 150 \text{ MeV}$  the two orders agree in the whole  $\mu_B / T$  range shown in the figure, at  $T = 160 \text{ MeV}$  the central line of the next-to-next-to-leading order bends upwards and is not contained in the next-to-leading order band. To make the NLO prediction precise substantially more computer time would be needed.

## 5 Conclusions and Outlook

In this manuscript, we have calculated several diagonal and non-diagonal fluctuations of electric charge, baryon number and strangeness up to sixth-order, in a system of 2+1+1 quark flavours with physical quark masses, on a lattice with size  $48^3 \times 12$ . The analysis has been performed simulating the lower order fluctuations at zero and imaginary chemical potential  $\mu_B$ , and extracting the higher order fluctuations as derivatives of the lower order ones at  $\mu_B = 0$ . The chemical potentials for electric charge and strangeness have both been set to zero in the simulations. From these fluctuations, we have constructed ratios of baryon number cumulants as functions of  $T$  and  $\mu_B$ , by means of a Taylor series which

takes into account the experimental constraints  $\langle n_S \rangle = 0$  and  $\langle n_Q \rangle = 0.4\langle n_B \rangle$ . These ratios qualitatively explain the behaviour observed in the experimental measurements by the STAR collaboration as functions of the collision energy.

We focused on observables (baryon distribution, ratios of cumulants) that are less sensitive to lattice artefacts. An obvious extension of our work will be the use of finer lattices and a continuum extrapolation. The other extension is to use a two- or even three-dimensional mapping of the space of the imaginary chemical potentials using non-vanishing  $\mu_S$  and  $\mu_Q$ . That would not only improve the  $\mu_S$ - and  $\mu_Q$ -derivatives, but would allow us to study the melting of states with various strangeness and electric charge quantum numbers. Our first study in this direction using strangeness chemical potentials was published in Ref. 25.

## Acknowledgements

This project was funded by the DFG grant SFB/TR55. The authors gratefully acknowledge the Gauss Centre for Supercomputing e.V. ([www.gauss-centre.eu](http://www.gauss-centre.eu)) for funding this project by providing computing time on the GCS Supercomputer JUQUEEN<sup>26</sup> at Jülich Supercomputing Centre (JSC) as well as on HAZELHEN at HLRS Stuttgart, Germany.

## References

1. A. Bazavov *et al.*, *Chiral crossover in QCD at zero and non-zero chemical potentials*, Phys. Lett. B **795**, 15–21, 2019.
2. C. Bonati, M. D’Elia, F. Negro, F. Sanfilippo, and K. Zambello, *Curvature of the pseudocritical line in QCD: Taylor expansion matches analytic continuation*, Phys. Rev. D **98**, 054510, 2018.
3. A. Bazavov *et al.*, *Skewness and kurtosis of net baryon-number distributions at small values of the baryon chemical potential*, Phys. Rev. D **96**, 074510, 2017.
4. R. V. Gavai and S. Gupta, *QCD at finite chemical potential with six time slices*, Phys. Rev. D **78**, 114503, 2008.
5. J. N. Guenther, R. Bellwied, S. Borsanyi, Z. Fodor, S. D. Katz, A. Pasztor, C. Ratti, and K. K. Szabó, *The QCD equation of state at finite density from analytical continuation*, Nucl. Phys. A **967**, 720–723, 2017.
6. M. D’Elia, G. Gagliardi, and F. Sanfilippo, *Higher order quark number fluctuations via imaginary chemical potentials in  $N_f = 2 + 1$  QCD*, Phys. Rev. D **95**, 094503, 2017.
7. C. R. Allton, S. Ejiri, S. J. Hands, O. Kaczmarek, F. Karsch, E. Laermann, C. Schmidt, and L. Scorzato, *The QCD thermal phase transition in the presence of a small chemical potential*, Phys. Rev. D **66**, 074507, 2002.
8. R. Bellwied, S. Borsanyi, Z. Fodor, S. D. Katz, A. Pasztor, C. Ratti, and K. K. Szabo, *Fluctuations and correlations in high temperature QCD*, Phys. Rev. D **92**, 114505, 2015.
9. A. Roberge and N. Weiss, *Gauge Theories With Imaginary Chemical Potential and the Phases of QCD*, Nucl. Phys. B **275**, 734–745, 1986.

10. V. Vovchenko, A. Pasztor, Z. Fodor, S. D. Katz, and H. Stoecker, *Repulsive baryonic interactions and lattice QCD observables at imaginary chemical potential*, Phys. Lett. B **775**, 71–78, 2017.
11. A. Vuorinen, *Quark number susceptibilities of hot QCD up to  $g^6 \ln g$* , Phys. Rev. D **67**, 074032, 2003.
12. C. Bonati, M. D’Elia, M. Mariti, M. Mesiti, F. Negro, and F. Sanfilippo, *Curvature of the chiral pseudocritical line in QCD: Continuum extrapolated results*, Phys. Rev. D **92**, 054503, 2015.
13. R. Bellwied, S. Borsanyi, Z. Fodor, J. Guenther, S. D. Katz, C. Ratti, and K. K. Szabo, *The QCD phase diagram from analytic continuation*, Phys. Lett. B **751**, 559–564, 2015.
14. P. Cea, L. Cosmai, and A. Papa, *Critical line of 2+1 flavor QCD: Toward the continuum limit*, Phys. Rev. D **93**, 014507, 2016.
15. A. Bazavov *et al.*, *The QCD Equation of State to  $\mathcal{O}(\mu_B^6)$  from Lattice QCD*, Phys. Rev. D **95**, 054504, 2017.
16. C. McNeile, C. T. H. Davies, E. Follana, K. Hornbostel, and G. P. Lepage, *High-Precision  $c$  and  $b$  Masses, and QCD Coupling from Current-Current Correlators in Lattice and Continuum QCD*, Phys. Rev. D **82**, 034512, 2010.
17. S. Borsanyi, Z. Fodor, J. N. Guenther, S. K. Katz, K. K. Szabo, A. Pasztor, I. Portillo, and C. Ratti, *Higher order fluctuations and correlations of conserved charges from lattice QCD*, JHEP **2018**, 205, 2018.
18. H. Akaike, *Information theory and an extension of the maximum likelihood principle*, in Selected Papers of Hirotugu Akaike, E. Parzen, K. Tanabe, G. Kitagawa (Editors), Springer, 119–213, 1998.
19. S. Dürr *et al.*, *Ab Initio Determination of Light Hadron Masses*, Science **322**, 1224–1227, 2008.
20. A. Bazavov *et al.*, *Freeze-out Conditions in Heavy Ion Collisions from QCD Thermodynamics*, Phys. Rev. Lett. **109**, 192302, 2012.
21. S. Borsanyi, Z. Fodor, S. D. Katz, S. Krieg, C. Ratti, and K. K. Szabo, *Freeze-out parameters: lattice meets experiment*, Phys. Rev. Lett. **111**, 062005, 2013.
22. X. Luo, *Energy Dependence of Moments of Net-Proton and Net-Charge Multiplicity Distributions at STAR*, PoS CPOD2014, 019, 2015.
23. J. Thäder, *Higher Moments of Net-Particle Multiplicity Distributions*, Nucl. Phys. A **956**, 320–323, 2016.
24. A. Andronic, P. Braun-Munzinger, and J. Stachel, *Hadron production in central nucleus-nucleus collisions at chemical freeze-out*, Nucl. Phys. A **772**, 167–199, 2006.
25. Paolo Alba *et al.*, *Constraining the hadronic spectrum through QCD thermodynamics on the lattice*, Phys. Rev. D, **96**, 034517, 2017.
26. M. Stephan, J. Docter, *JUQUEEN: IBM Blue Gene/Q Supercomputer System at the Jülich Supercomputing Centre*, JLSRF **1**, A1, 2015.